RSC Advances

ROYAL SOCIETY OF CHEMISTRY

www.rsc.org/advances

Effect of bauxite additive on the ash sintering characteristics during K_2CO_3-catalyzed steam gasification of lignite

Jiguang Zhang[a], Li Zhang[a*], Zhongqing Yang[a], Yunfei Yan[a], Yandong Mao[b], Jicheng Bi[b]

[a] Key Laboratory of Low-grade Energy Utilization Technologies and Systems, Ministry of Education of PRC, Chongqing University, 174 Shazheng Street, Shapingba District, Chongqing, 400044, China

[b] State Key Laboratory of Coal-Based Low Carbon Energy, ENN Energy Technology Development Pty Ltd, Huaxiang Road, Langfang City, Hebei Province, 065001, China

This paper is aimed to investigate the ash sintering characteristics of LLI lignite with bauxite additive during K_2CO_3-catalyzed steam gasification. In this paper, the ash samples were prepared using a catalytic gasification system at 1123 K under steam atmosphere with carrier gas N_2. The ash sintering temperature was determined using a pressure-drop sintering device with inert N_2. The ash mineralogy and morphology were analyzed using an X-ray diffractometer (XRD) and a scanning electron microscope-energy dispersive X-ray spectrometer (SEM-EDS). The results showed that K_2CO_3 decreased the sintering temperatures of ash samples and made the ash molten degree become more serious. Kaliophilite was the main cause to facilitate the formation of liquid phases and trigger the occurrence of sintering, resulting in a lower ash sintering temperature. In addition, the addition of bauxite could ease the molten degree of ashes and lead to a higher ash sintering temperature. The main cause is that bauxite including sufficient SiO_2 and Al_2O_3 could react with other minerals to generate more refractory silicon oxide and diminish the fluxing

[*] Corresponding Author

Telephone: +86- 23-65105655; Fax: +61- 23-65102473. E-mail: lizhang@cqu.edu.cn (Li Zhang).

arcanite and amorphous materials in ashes. At last, from the view of mineralogy, the addition of bauxite also can decrease the gasification rate of lignite by reacting with potassium to generate water-insoluble kaliophilite and deactivating the potassium catalyst.

Keywords: Ash sintering temperature; Bauxite; Potassium carbonate; Catalytic gasification; Lignite

1. INTRODUCTION

Currently, coal is the main energy resource in China, which occupies about 70% of the total energy consumption [1, 2]. About 12.7% of the total coal reserves are covered by lignite [3, 4]. As a efficient and clean lignite utilization method, the catalytic gasification technology has been paid much attention and is widely employed [5, 6]. It is well known that alkali and alkaline earth metal (AAEM) elements of lignite acting as a catalyst play a significant role in the lignite gasification process [7, 8]. However, AAEM species can potentially give rise to some undesirable effects and issues relating with the ash in gasifiers [9, 10]. These issues including bed agglomeration, slagging, corrosion, erosion and so on majorly originate from the sintering behavior [11, 12]. Hence, it is necessary to study the sintering characteristics of lignite ash produced by catalytic gasification.

Ash sintering refers to the process in which some partial melting particles become sticky and bond together with adjacent solid particles. These bonded particles will potentially grow up and finally form a bulk of ash deposits [13]. Literature reports have reached consensus that the ash sintering behavior is mainly controlled by the ash chemistry and other factors such as atmosphere, temperature, pressure, and particle size [8, 10, 14]. Jing et al. [15] investigated the effect of ash composition on the sintering behavior during pressurized combustion and

gasification process using SEM and XRD technique. The result showed that the addition of Fe_2O_3 can obviously reduce the sintering temperatures under gasification atmospheres and only slightly affect the sintering temperature under combustion atmosphere. Matjie et al. [16] studied the behavior of coal mineral matter in sintering and slagging of ash during the gasification process using quantitative XRD and automated electron beam image analysis. The results indicated that the minerals and inorganic elements in the coal have undergone significant transformations during gasification, the nature of which depends not only on the mineralogy but also the mineral association. Minerals and mineral associations were responsible for ash sintering behavior.

Generally, the AAEM (e.g. potassium) is easily to react with Si and Al compounds in coal ash, and then somewhat resulting in the formation of lower melting point products [17-19]. Potassium can be incorporated into the structures of sil.icates to form eutectics with low melting temperatures of about 813 - 873 K in the K_2O-SiO_2 binary system [20]. Potassium can also facilitate the formation of low temperature eutectics (973 - 1273 K) in the K_2O-SiO_2-Al_2O_3 ternary systems [21]. In addition, bauxite, a naturally occurring heterogeneous ore, is the world's main source of aluminum [22]. One of conventionally commercial applications of bauxite is refractory, which is an active additive for preventing the formation of problematic ash components [23]. The bauxite can trap the alkali (particularly potassium) into the solid [24, 25]. Barisano, D et al. [26] reported that at gasification steady state condition, the addition of bauxite as a sorbent can remove the potassium vapor and a gradual and significant decrease in the K concentration was observed. After high temperature treatment, the bauxite including aluminum-bearing minerals can capture the potassium to generate some higher melting point of alumina with different crystal structures [27, 28]. However, although the bauxite additive gives rise to increase the ash fusion temperature, it somewhat leads to the deactivation of

potassium catalyst. Thus, it needs to be better understand in ash minerals related problems of lignite with the addition of bauxite during K_2CO_3-catalyzed steam gasification.

However, studies on the ash sintering characteristics of lignite with different concentrations of bauxite additive produced by different concentrations of K_2CO_3 catalytic gasification are scarce. Accordingly, a systematic research effort is needed to better understand the interactions among lignite minerals, K_2CO_3 and bauxite during catalytic gasification condition and how the ash sintering characteristics are impacted upon. To this end, the current study investigated the effect of bauxite additive on the ash sintering characteristics during K_2CO_3-catalyzed gasification of lignite.

2. EXPERIMENTAL SECTION

In this work, a lignite named LLI from China was selected. The lignite sample was pulverized and sieved to less than 0.2 mm in size. According to the Chinese standard (GB/T212-2001), the lignite ash was prepared by heating the lignite sample in air in a Muffle furnace to 1088 K for 2 hours. The ash chemical compositions of LLI lignite were analyzed using X-ray fluorescence (XRF) and the results as well as the proximate and ultimate analysis data of LLI lignite are presented in Table 1. The ash fusion temperatures of ash samples were tested under air atmosphere according to the Chinese standard (GB219-74) and the results are also shown in Table 1.

To investigate the influence of additive on the ash sintering behavior, the bauxite was chosen for this study in respect of its high content of refractory Al_2O_3 and SiO_2. The ingredients of bauxite were tested by XRD technique and the results are presented in Table 2. Besides, as

for catalytic gasification, K_2CO_3 regarded as one of the most promising catalyst for coal gasification was selected in this work. The mass fractions of K_2CO_3 or bauxite, i.e., K_2CO_3 (or bauxite)/lignite were set to 0%, 1%, 5% and 10%. The bauxite and K_2CO_3 both were added to the lignite sample using an impregnation method. After thorough mixing by vigorous stirring, the samples were dried in an oven at 378 K for 24 hours. At last, the dried samples were mechanically stirred adequately in a crucible again in order to mixing the additives and lignite evenly.

During the process of catalytic gasification, the gasification agent gas was steam. The steam volume flow rate was controlled by a water pump. The carrier gas was N_2, which had the same rate of volume flow of 500 cm^3 min^{-1} as steam. The carrier gas could give impetus to the steam to flow from bottom to top of the fixed-bed gasification reactor (500mm length and 50mm OD and 36mm ID). The whole gasification reactor was heated by a vertical electric furnace to guarantee that steam and reactor maintained a desired temperature. Firstly, a sample of approximately 4g was placed in the gasification reactor. Secondly, let the N_2 get into the reactor and increased the furnace temperature to 1123K and then kept the temperature for 5 mins for lignite pyrolysis before gasification process. At last, opened the water pump to give a source to generate steam for steam gasification and then kept the whole system for 4 hours to make sure that the samples were gasified fully.

After the ash preparation process, a pressure-drop sintering device was used to determine the ash sintering temperature in inert N_2 atmosphere. A schematic diagram of the pressure-drop sintering device is shown in Figure 1. Briefly, an ash pellet (8mm diameter and height) of approximately 0.4g, prepared using an ash pellet compaction device with a compaction pressure of 25 MPa, was inserted in the middle of alumina mullite tube (1000mm length and

8mm OD and 5mm ID) in an electric furnace. A stream of inert N_2 passed through the pellet at a constant flow rate of 4 cm^3 min^{-1} controlled by a mass flow controller. The furnace was heated from ambient temperature at 8 K min^{-1} and the pressure-drop across the pellet was recorded as a function of the temperature. In the current experimentation, the ash sintering temperature was defined as the temperature when the pressure-drop across the pellet reached to the maximum [29]. The sintering temperatures thus determined using this technique had a repeatability of ± 10 K.

In order to understand the reasons for the changes in the ash sintering behavior and clarify the cause of the occurrence of ash sintering due to the different ash preparation procedures, the morphological and mineralogical transformation of the ash samples were investigated. The morphological characteristics and spot composition analysis were performed using a TESCAN-Vega-3-XM scanning electronic microscopy (SEM) analyzer aided with an Oxford X-ray energy dispersive spectroscopy (EDS). The spot location is represented on the provided SEM images by a star symbol. To gain a better understanding of the ash mineralogical transformations and characteristics, ash samples were studied using a PANalytical X-ray diffractometer analyzer (EMPYREAN) with copper Kα radiation. The qualitative powder XRD analysis employed an accelerating voltage of 40 kV, a current of 40 mA and a scan speed of 0.0847 $°s^{-1}$ between 5° and 70° of the 2θ.

3. RESULTS AND DISCUSSION

3.1 Effect of K_2CO_3 and bauxite on the ash sintering temperature

In order to study the effect of K_2CO_3 and bauxite on the ash sintering temperature, Figure 2 compared the ash sintering temperature of LLI lignite with different concentrations of bauxite additive produced by different concentrations of K_2CO_3 catalytic gasification.

For the effect of K_2CO_3 on the ash sintering temperature, with a same concentration of bauxite additive, it is seen that the sintering temperatures of ash samples decreased by increasing the concentration of K_2CO_3 from 0 to 10 wt%; the ashes from LLI without K_2CO_3 catalyst showed the highest sintering temperatures, whereas the ashes from LLI with 10 wt% K_2CO_3 had the lowest sintering temperatures. Besides, it is also noted that, without bauxite additive, the ash sintering temperature difference between LLI with and without 10 wt% K_2CO_3 was relatively larger than others, and the decreased degree was about 149 K. At last, these phenomena demonstrated that K_2CO_3 could play a significant role in reducing ash sintering temperature.

Meanwhile, for the effect of bauxite additive on the ash sintering temperature, Figure 2 also showed that, with a same concentration of K_2CO_3 catalyst and the concentration of bauxite raised from 0 to 10 wt%, the sintering temperatures of ash samples got increased; the ashes from LLI without bauxite additive showed the lowest sintering temperatures, whereas the ashes from LLI with 10 wt% bauxite additive had the highest sintering temperatures. In addition, it is also illustrated that, with 10 wt% concentration of K_2CO_3 catalyst, the ash sintering temperature difference between LLI with and without bauxite additive was relatively larger than others, and the increased sintering temperature was about 82 K. These phenomena verified that bauxite could play an important role in promoting ash sintering temperature.

3.2 Ash morphology

3.2.1 Effect of K_2CO_3

Figure 3 illustrated the ash surface morphology change of LLI lignite with different concentrations of bauxite additive produced by different concentrations of K_2CO_3. In Figure 3, the second row including four images presents four ash samples from LLI with 1 wt% bauxite additive. On the left of first row, it is shown that the ash samples from LLI without K_2CO_3 catalyst present some irregularly shaped and dispersed particles, in which no obvious melting or agglomeration phenomena occurred. By increasing the concentration of K_2CO_3 catalyst to 5 wt%, still no clear molten phenomenon occurred on the ash particle surfaces. However, when the concentration of K_2CO_3 was up to 10 wt%, the ash particles hold together and became agglomerated, the surface of which was obviously molten and smooth, which indicated that some liquid phases had already formed and the ash sintering had occurred. On the whole, the morphology changes validated the trend of ash sintering temperature results in Figure 2. Besides, from the analysis of EDS, the ash samples from LLI without K_2CO_3 catalyst, the chosen spot on the particle was mainly composed of O, Ca, Si and Al, implying that the particle may contain Ca-bearing aluminosilicate including feldspar minerals. With the increase of K_2CO_3, higher content of K element presented in the elemental analysis. When the concentration of K_2CO_3 was 10 wt%, the EDS results showed that those melting surfaces were mainly comprised of O, K, Si, and Al, indicating that the melting surface may have been comprised of K-bearing aluminosilicate. It has been reported that K-bearing aluminosilicate could react with other minerals to form the low temperature eutectics, which facilitated the formation of liquid phases. Those liquid phase could potentially act as a glue that bonded the ash particles together in a mechanism called the viscous flow sintering [13].

Likewise, from third or fourth row of Figure 3, it is shown that with 5 wt% or 10 wt% bauxite additives, the morphology change and elemental analysis of ash particles showed correspondingly similar trend with the four ash samples from LLI with 1wt% bauxite as the rise of K_2CO_3 concentration, respectively. The trend was that irregularly shaped and dispersed particles tended to be agglomerated particles with molten and smooth surfaces, and the molten degree became more severe. In addition, with a higher concentration of K_2CO_3, the EDS results showed that those melting surfaces were mainly comprised of O, Si, K and Al, implying K-bearing aluminosilicate played an important role in facilitating the melting surface. Overall, the increase of K_2CO_3 promoted the content of K-bearing aluminosilicate in ash, which facilitated the formation of liquid phases and the occurrence of ash sintering.

3.2.2 Effect of bauxite

In Figure 3 also illustrated the effect of bauxite additive on the ash surface morphology change. The first column including four images presents four ash samples from LLI without K_2CO_3 catalyst. All these ash samples showed irregularly shaped particles without melting surface, which confirmed the results that these ash samples had high ash sintering temperatures which were above 1133 K and exceeded the ash preparation temperature of 1123 K shown in Figure 2. Thus, it is difficult to distinguish and compare the melting degree of these ash samples by surface morphology. By the analysis of EDS, the elemental compositions on the surface of these unmelted particles were mainly O, Si, Al and Ca, indicating that these particles may be composed of Ca-containing feldspar minerals. Similarly, the second column including four images presents four ash samples from LLI with 1 wt% K_2CO_3 catalyst. From Figure 3, it is shown that with the concentration of 1 wt% K_2CO_3 catalyst, the morphology change and elemental analysis of ash particles was correspondingly

similar with the four ash samples from LLI without K_2CO_3 catalyst as the rise of bauxite concentration, respectively. This can be explained by the K_2CO_3 proportion was only 1 wt%, which was not enough to largely impact on ash mineral transformation and morphology change.

Additionally, with the same concentration of 5 wt% K_2CO_3, the surface texture of four kinds of ash particles in the third column of Figure 3 were still irregularly shaped and unmelted as the augment of bauxite additive from 0 wt% to 10 wt%. At last, when the concentration of K_2CO_3 was added up to 10 wt%, the four kinds of ash particles in the fourth column of Figure 3 were obvious agglomerated and sticked together with molten surfaces. The occurrence of molten surface indicated that some liquid phases had formed. Those liquid phases could act as glues bonding particles together for the viscous flow sintering [30]. Meanwhile, the melting degree of ashes from LLI without the addition of bauxite which presented the neck of sintered ash particles was much more serious than the others. In other words, as the augment of bauxite additive, it is also illustrated that the molten degree of ash samples was eased, which was consistent with increasing sintering temperature of ash samples shown in Figure 2. In addition, due to the addition of 10 wt% K_2CO_3, the EDS result showed that the major elemental compositions of melting surface of all four ash samples were composed of O, K, Si, Al and Fe, in which high content of K and Fe elements existed. The existence of iron element was originated from the addition of bauxite. It is suggested that the melting surface may have been comprised of K-bearing aluminosilicate and Fe-containing compounds. These K-bearing aluminosilicate and Fe-containing compounds were capable of forming low melting temperature eutectics and then facilitated the occurrence of ash sintering [31].

3.3 Ash mineralogy

3.3.1 Effect of K_2CO_3

Figure 4 presents the XRD patterns of the ashes of LLI lignite with 1 wt% bauxite additive produced by different concentrations of K_2CO_3 catalytic gasification at 1123 K. In Figure 4, the results showed that the main minerals were silicon oxide (SiO_2), nosean ($Na_{8.08}(Al_6Si_6O_{24})(SO_4)_{0.98}$), iron oxide ($Fe_3O_4$), anorthoclase ($(Na,K)(Si_3Al)O_8$) and albite ($NaAlSi_3O_8$) in the ash from LLI lignite. Except silicon oxide, these are fluxing minerals [31] which are prone to produce low-temperature co-fusion with other minerals [15]. As the increase of the K_2CO_3 concentration, new K-containing phases arcanite (K_2SO_4), leucite ($KAlSi_2O_6$) and kaliophilite ($KAlSiO_4$) appeared while the content of silicon oxide became less and feldspars such as nosean disappeared. The arcanite was formed as a product from the reaction that potassium was adsorbed by SO_3 [32]. The kaliophilite started to appear in the ash sample from LLI lignite produced by catalytic gasification with 5 wt% K_2CO_3, then increased in the content when the proportion of K_2CO_3 enhanced up to 10 wt%. The kaliophilite which is a kind of K-bearing aluminosilicate was formed as a reaction product from K element which partly from arcanite, SiO_2 and Al_2O_3 [33]. The kaliophilite and leucite which are members of the feldspathoid group of minerals and arcanite all can react with other minerals to form low temperature eutectics [34], leading to the decrease of the ash sintering temperature. Meanwhile, this verified the analysis of SEM-EDS in the Figure 3 that the melting surface of ash samples was comprised of K-bearing aluminosilicate. And these K-bearing aluminosilicate may include the kaliophilite and some co-fusion mixtures. Besides, when the proportion of K_2CO_3 enhanced up to 10 wt%, it is illustrated that there was a broad hump existing at $2\theta=33°$ in the diffraction pattern, which suggests that some amorphous materials existed in the ash sample. The XRD technique can not detect which kind of mineral is in the amorphous materials, but

can estimate the content of amorphous materials. Those amorphous materials mainly contained some low temperature co-fusions [35]. Overall, the presence of K-containing compounds (arcanite and kaliophilite) and amorphous materials led to a lower ash sintering temperature. The similar phenomena were also observed for the other ash samples of LLI lignite with 5 wt% bauxite additive produced by different concentrations of K_2CO_3 catalytic gasification.

In addition, Figure 5 demonstrates that the XRD patterns of the ashes of LLI lignite with 10 wt% bauxite additive produced by different concentrations of K_2CO_3 catalytic gasification. It is evident that the major minerals of ashes produced from LLI lignite without K_2CO_3 at 1123 K were silicon oxide, nosean, iron oxide and gehlenite ($Ca_2Al(AlSi)O_7$). Similarly, by increasing the K_2CO_3 concentration to 10 wt%, the major mineral in the ash was fluxing kaliophilite while feldspars such as gehlenite disappeared. Compared with the results in Figure 4, it is noted that less arcanite presented in the ash samples from LLI lignite 10wt% K_2CO_3 in Figure 5. This is because the bauxite had a strong affinity to K_2CO_3. The potassium could start to be captured to generate the kaliophilite by the kaolin which was a part of bauxite even at 673K [36]. As the analysis from Figure 4, kaliophilite could react with other minerals to form low temperature eutectics [34]. On the whole, the existence of massive kaliophilite was the main cause to lead to a lower ash sintering temperature.

3.3.2 Effect of bauxite

Figure 6 illustrates the XRD patterns of the ashes of LLI lignite with different concentrations of bauxite additive produced by gasification. The results showed that the main minerals were silicon oxide, nosean and iron oxide in the ash from LLI lignite. As increasing the bauxite

addition, the peak intensity of refractory silicon oxide in the pattern was significantly increased, suggesting that the content of silicon oxide became richer in the ash samples. In addition, some feldspar minerals such as nosean and albite-calcian appeared and significantly increased in the content in the ashes. These are because the fact that the increased bauxite including sufficient SiO_2 and Al_2O_3 could react with other minerals in the ashes to generate those feldspar minerals [37]. These results correlated with the analysis of SEM-EDS that some irregularly shaped particles were composed of feldspar minerals. Therefore, it is concluded that the increased content of refractory silicon oxide reduced the proportion of fluxing minerals in the ashes, which somewhat promoted the ash sintering temperature. The similar phenomena were also detected for the other ash samples of LLI lignite with different concentrations of bauxite additive produced by catalytic gasification with 1 wt% or 5 wt% K_2CO_3.

Furthermore, this study also investigated the XRD patterns of ashes of LLI lignite with different concentrations of bauxite additive produced under catalytic gasification with 10wt% K_2CO_3. As it can be observed in Figure 7, with the concentration of 10 wt% K_2CO_3, the major minerals in the ash from LLI lignite without bauxite addition were silicon oxide, kaliophilite, arcanite and potassium calcium silicate ($K_4CaSi_3O_9$). Likewise, as the rise of bauxite addition from 1 to 10 wt%, it is noted that the contents of iron oxide and silicon oxide were slightly increased while arcanite became less in the ashes. This is because the fact that the increased bauxite brought in increasing silicon oxide and iron oxide. The iron oxide was transformed from ferric oxide containing in bauxite during reducing steam atmosphere [38], which could not largely impact on the sintering temperature due to the degree of variability of iron oxide was slightly. The potassium was captured to generate the kaliophilite instead of arcanite by the bauxite addition, which is similar with the XRD analysis above. These

phenomena are consistent with the results in the fourth column of Figure 3. Moreover, it is also observed that there was a broad hump existing at 2θ=33° in the diffraction pattern of four ash samples, respectively, implying that each ash sample contained some amorphous materials. The area under the hump depends on the content of amorphous materials in the sample. It is believed that bigger area means higher content of amorphous materials in the sample [35]. However, it is illustrated that the area became smaller as the addition of bauxite increased from 0 to 10 wt%, demonstrating that the amount of amorphous materials containing low temperature co-fusions in the samples was reduced. Therefore, together these factors including increased refractory silicon oxide, less fluxing arcanite and decreased amorphous materials promoted the ash sintering temperature.

In addition, it is stated that a key factor of catalytic gasification is to make sure the activity of catalyst, which majorly determines the carbon conversion and gasification rate of lignite [39]. In this study, the existence of potassium catalyst which can possess the catalytic function for gasification mainly are water-soluble K_2CO_3 and arcanite [40]. However, due to the presence of bauxite, it can react with the active K_2CO_3 to form water-insoluble compound kaliophilite instead of arcanite, leading to the deactivation of potassium catalyst [41]. Thus, with a same concentration of K_2CO_3, the less content of arcanite indicates lower activity of catalyst and gasification rate of lignite, and vice versa. In Figure 7, as the rise of bauxite addition, it is illustrated that the content of arcanite were decreased and the proportion of kaliophilite increased in ashes, which suggests that the addition of bauxite can decrease the gasification rate of lignite.

The ash sintering was triggered by the formation of viscous liquid phases on the ash particles surface [13, 42]. The viscous liquid phases further lead to rearrangement and agglomeration of

ash particles [43]. Therefore, the key factor of the occurrence of sintering is the presence of liquid phases. Usually, the liquid phases originated from some low-temperature co-fusions. In this study, these low-temperature co-fusions were produced by some interactions between additives and lignite minerals. Based on the above analysis in this study, due to the presence of potassium, on the one hand, it could react with SO_3 from lignite to generate fluxing arcanite (K_2SO_4); on the other hand, it is easy to react with SiO_2 and Al_2O_3 from bauxite and lignite to produce some K-containing phases leucite ($KAlSi_2O_6$) and kaliophilite ($KAlSiO_4$). Leucite and kaliophilite which are members of the feldspathoid group of minerals and fluxing arcanite could react with other minerals to form low temperature eutectics and then resulted in the generation of liquid phases and the occurrence of ash sintering. The main reactions involving with LLI lignite minerals, K_2CO_3 and bauxite during catalytic gasification discussed before are shown as Table 3.

As a whole, as increasing the bauxite concentration, the addition bauxite can retard the occurrence of sintering and lead to a higher ash sintering temperature by the way of generating more refractory silicon oxide and diminishing the fluxing arcanite and amorphous materials in ash. In addition, the addition of bauxite can decrease the gasification rate of lignite by forming water-insoluble kaliophilite with K_2CO_3 and deactivating the potassium catalyst.

4. CONCLUSIONS

In this work we have investigated the ash sintering characteristics and ash minerals transformation of LLI lignite with bauxite additive during K_2CO_3-catalyzed steam gasification at 1123 K using SEM-EDS and XRD. As increasing the K_2CO_3 concentration,

K_2CO_3 decreased the sintering temperatures of ash samples and made the ash molten degree become more serious. The kaliophilite generated by the interactions between potassium and aluminosilicate was the main cause to facilitate the formation of liquid phases and trigger the occurrence of sintering, resulting in a lower ash sintering temperature. On the other hand, with increasing the concentration of bauxite additives from 0 to 10 wt% the sintering temperatures of ash samples got promoted. Besides, the melting surfaces of ash particles were comprised of kaliophilite and iron oxide. The addition of bauxite can ease the molten degree of ashes and lead to a higher ash sintering temperature. The main cause is that bauxite including sufficient SiO_2 and Al_2O_3 could react with other minerals to generate more refractory silicon oxide and diminish the fluxing arcanite and amorphous materials in ashes. At last, from the view of mineralogy, the addition of bauxite also can decrease the gasification rate of lignite by reacting with potassium to generate water-insoluble kaliophilite and deactivating the potassium catalyst. These results could provide a useful support for the practical application of K_2CO_3-catalyzed steam gasification.

ACKNOWLEDGMENT

The authors would like to thank the financial supports of Natural Science Foundation of China with Project No.51206200, and the Fundamental Research Funds for the Central Universities with Project No. CDJZR12140031. Jiguang Zhang also acknowledges the scholarships provided by the China Scholarships Council and Centre for Energy in The University of Western Australia.

REFERENCES

1 Z. Song and C. Kuenzer, *International Journal of Coal Geology*, 2014, **133**, 72-99.

2 X. Yang, C. Zhang, P. Tan, T. Yang, Q. Fang and G. Chen, *Energ Fuel*, 2013, **28**, 264-274.

3 Y. Zhao, J. Zhang and C. Zheng, *Fuel*, 2013, **109**, 86-93.

4 F. Li, J. Huang, Y. Fang and Y. Wang, *Energ Fuel*, 2010, **25**, 273-280.

5 J. Oexmann, C. Hensel and A. Kather, *International Journal of Greenhouse Gas Control*, 2008, **2**, 539-552.

6 M. A. Nahil, X. Wang, C. Wu, H. Yang, H. Chen and P. T. Williams, *RSC Advances*, 2013, **3**, 5583-5590.

7 R. Liu, W. Zhao, T. Zhang, L. Yang, Z. Zhou and S. Qi, *RSC Advances*, 2014, **4**, 39463-39471.

8 R. Habibi, J. Kopyscinski, M. S. Masnadi, J. Lam, J. R. Grace, C. A. Mims and J. M. Hill, *Energ Fuel*, 2012, **27**, 494-500.

9 L. Liu, H. Liu, M. Cui, Y. Hu and J. Wang, *Fuel*, 2013, **112**, 687-694.

10 J. Wang, K. Sakanishi, I. Saito, T. Takarada and K. Morishita, *Energ Fuel*, 2005, **19**, 2114-2120.

11 M. T. C. Tangsathitkulchai, *Fuel Process Technol*, 2001, **72**, 163-183.

12 H. Atakül, B. Hilmioğlu and E. Ekinci, *Fuel Process Technol*, 2005, **86**, 1369-1383.

13 B. Jung and H. H. Schobert, *Energ Fuel*, 1991, **5**, 555-561.

14 N. J. Jing, Q. H. Wang, L. M. Cheng, Z. Y. Luo and K. F. Cen, *Fuel*, 2013, **103**, 87-93.

15 N.-j. Jing, Q.-h. Wang, Y.-k. Yang, L.-m. Cheng, Z.-y. Luo and K.-f. Cen, *Journal of Zhejiang University SCIENCE A*, 2012, **13**, 230-238.

16 R. H. Matjie, D. French, C. R. Ward, P. C. Pistorius and Z. Li, *Fuel Process Technol*, 2011, **92**, 1426-1433.

17 J. R. Pullen, *IEA Coal Research*, 1984.

18 M. S. Masnadi, R. Habibi, J. Kopyscinski, J. M. Hill, X. Bi, C. J. Lim, N. Ellis and J. R. Grace, *Fuel*, 2014, **117, Part B**, 1204-1214.

19 e. a. Yu, *Bioresource Technology*, 2014.

20 L. Wang, J. E. Hustad and M. Grønli, *Energ Fuel*, 2012, **26**, 5905-5916.

21 X. Wu, Z. Zhang, G. Piao, X. He, Y. Chen, N. Kobayashi, S. Mori and Y. Itaya, *Energ Fuel*, 2009, **23**, 2420-2428.

22 K.-Y. Ling, X.-Q. Zhu, H.-S. Tang, Z.-G. Wang, H.-W. Yan, T. Han and W.-Y. Chen, *Ore Geology Reviews*, 2015, **65, Part 1**, 84-96.

23 W. Liu, J. Yang and B. Xiao, *International Journal of Mineral Processing*, 2009, **93**, 220-231.

24 A. Kosminski, D. P. Ross and J. B. Agnew, *Fuel Process Technol*, 2006, **87**, 1051-1062.

25 S. Roy and A. K. Saroha, *RSC Advances*, 2014, **4**, 56838-56847.

26 D. Barisano, C. Freda, F. Nanna, E. Fanelli and A. Villone, *Bioresource Technology*, 2012, **118**, 187-194.

27 G. H. Bai, W. Teng, X. G. Wang, J. G. Qin, P. Xu and P. C. Li, *T Nonferr Metal Soc*, 2010, **20**, S169-S175.

28 M. A. Gomez, M. J. Hendry, S. Elouatik, J. Essilfie-Dughan and S. Paikaray, *RSC Advances*, 2014, **4**, 54973-54988.

29 G. W. B. A. Y. Al-Otoom, L. K. Elliott, B. J. Skrifvars, M. Hupa, and T. F. Wall, *Energ Fuel*, 2000,, **14**, 227-233.

30 B. Jung and H. H. Schobert, *Energ Fuel*, 1992, **6**, 59-68.

31 N. Jing, Q. Wang, Z. Luo and K. Cen, *Fuel*, 2011, **90**, 2645-2651.

32 J. W. Nowok, J. P. Hurley and S. A. Benson, *J I Energy*, 1996, **69**, 12-14.

33 G. Bruno, L. Carvani and G. Passoni, *Fuel*, 1986, **65**, 1473-1475.

34 S. K. Gupta, R. P. Gupta, G. W. Bryant and T. F. Wall, *Fuel*, 1998, **77**, 1195-1201.

35 M. Tiainen, J. Daavitsainen and R. S. Laitinen, *Energ Fuel*, 2002, **16**, 871-877.

36 M. Jiang, J. Hu and J. Wang, *Fuel*, 2013, **109**, 14-20.

37 S. Konsomboon, S. Pipatmanomai, T. Madhiyanon and S. Tia, *Applied Energy*, 2011, **88**, 298-305.

38 X. Wu, Z. Zhang, Y. Chen, T. Zhou, J. Fan, G. Piao, N. Kobayashi, S. Mori and Y. Itaya, *Fuel Process Technol*, 2010, **91**, 1591-1600.

39 M.-Q. Jiang, R. Zhou, J. Hu, F.-C. Wang and J. Wang, *Fuel*, 2012, **99**, 64-71.

40 Y.-K. Kim, L.-f. Hao, J.-I. Park, J. Miyawaki, I. Mochida and S.-H. Yoon, *Fuel*, 2012, **94**, 516-522.

41 L. Klopper, C. A. Strydom and J. R. Bunt, *Journal of Analytical and Applied Pyrolysis*, 2012, **96**, 188-195.

42 A. Y. Al-Otoom, L. K. Elliott, B. Moghtaderi and T. F. Wall, *Fuel*, 2005, **84**, 109-114.

43 B.-J. S. a. M. Hupa, *Ind. Eng. Chem. Res*, 1992, **31**, 1026-1030.

List of Tables

Table 1

Table 1 Proximate and ultimate analysis and ash composition as well as ash fusion temperatures of LLI lignite

Proximate analysis / wt % (dry basis)			Ultimate analysis / wt % (dry basis)				
V	A	FC	C	H	O	N	S
32.54	15	52.46	67.18	1.76	17.66	0.68	4.27

Ash composition / wt %						
SiO	Al_2O	Fe_2O	CaO	Na_2O	K_2O	SO_3
44.3	17	10.2	11.4	1.51	1.61	10.8

Ash fusion temperatures (K) (oxidizing atmosphere)			
DT	ST	HT	FT
1305	1576	1614	1628

Table 2

Table 2 Ingredients of bauxite

Ingredients	wt %
Silica crystalline – quartz	<3
Kaolinite	1 – 20
Ferric oxide	1 – 20
Aluminium hydroxide	40 – 85

Table 3

Table 3 The main reactions involving with LLI lignite minerals, K_2CO_3 and bauxite during catalytic gasification under steam atmosphere at 1123 K

$K_2CO_3 + SO_3 \rightarrow K_2SO_4$（Arcanite）	(1)
$Al_2O_3 + SiO_2 + Na_2O + K_2O \rightarrow (Na,K)Al(Si_3,Al)O_8$ (Anorthoclase)	(2)
$Al_2O_3 + SiO_2 + Na_2O + CaO \rightarrow (Na,Ca)Al(Si,Al)_3O_8$ (Albite – Calcian)	(3)
$K_2CO_3 + Al_2O_3 + SiO_2 \rightarrow KAlSiO_4$ (Kaliophilite)	(4)
K_2SO_4(Arcanite) $+ Al_2O_3 + SiO_2 \rightarrow KAlSiO_4$ (Kaliophilite)	(5)

List of Figures

Figure 1

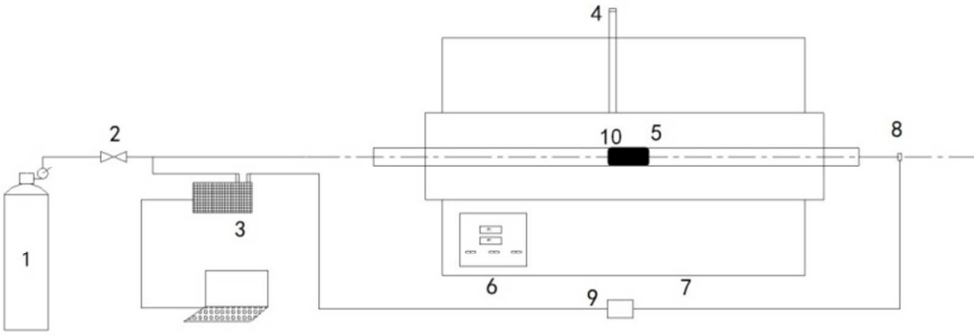

Figure 1 A schematic diagram of the pressure-drop sintering device (1: Gas cylinder; 2: Mass flow controller; 3: Data taker; 4: Thermocouple measuring furnace temperature; 5: Mullite tube; 6: Control panel; 7: Electric furnace; 8: Thermocouple measuring sample temperature; 9: Pressure transmitter; 10: Ash pellet)

Figure 2

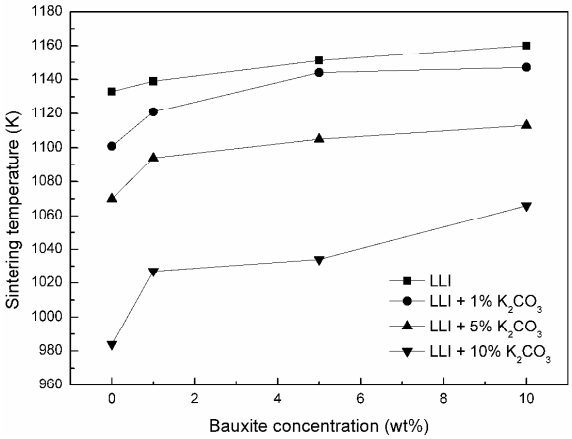

Figure 2 The ash sintering temperature of LLI lignite with different concentrations of bauxite additive produced by different concentrations of K_2CO_3 catalytic gasification at 1123 K under steam atmosphere

Figure 3

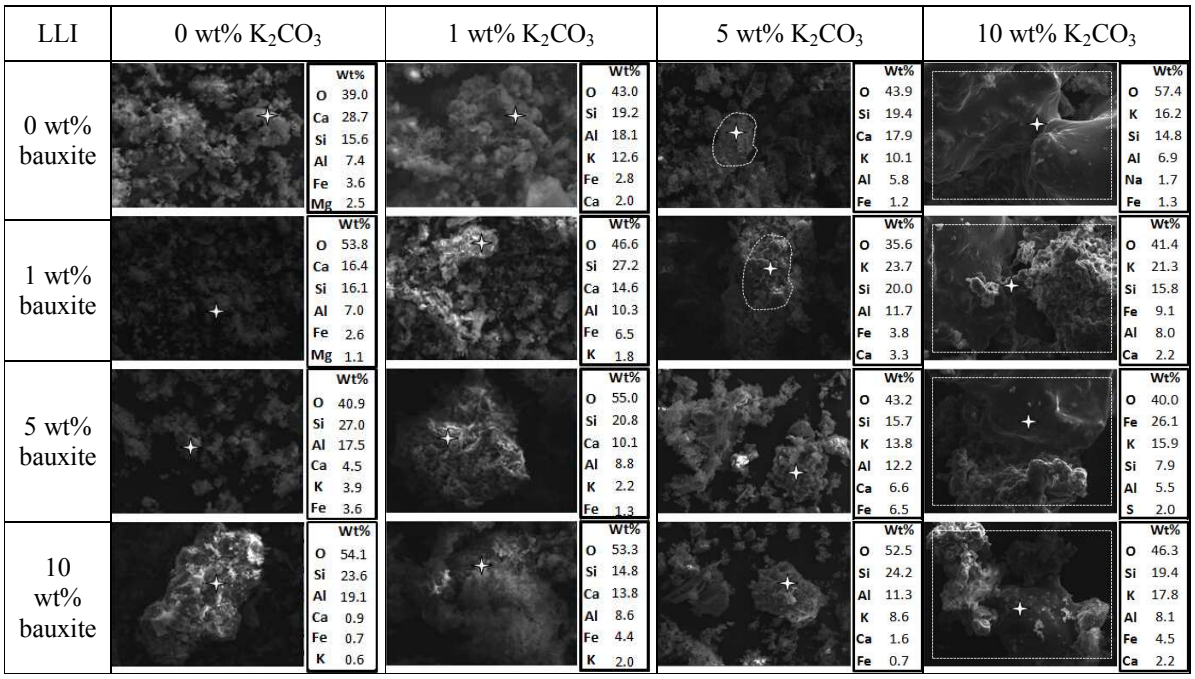

Figure 3 The SEM-EDS of the ashes of LLI lignite with different concentrations of bauxite additive produced by different concentrations of K_2CO_3 catalytic gasification at 1123 K under steam atmosphere (The magnification is 2 kx and scale bar for each image is 20 μm, the melting surface was surrounded by dotted line)

Figure 4

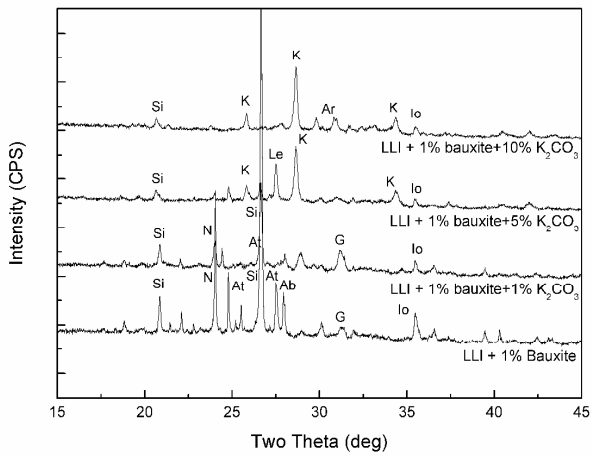

（Si - Silicon oxide (SiO_2); Io - Iron oxide (Fe_3O_4); K – Kaliophilite ($KAlSiO_4$); N - Nosean ($Na_{8.08}(Al_6Si_6O_{24})(SO_4)_{0.98}$); G - Gehlenite ($Ca_2Al(AlSi)O_7$); Ar – Arcanite ($K_2SO_4$); At - Anorthoclase ($(Na,K)(Si_3Al)O_8$); Ab - Albite ($NaAlSi_3O_8$); Le - Leucite ($KAlSi_2O_6$)）

Figure 4 The XRD patterns of the ashes of LLI lignite with 1 wt% bauxite additive produced by different concentrations of K_2CO_3 catalytic gasification at 1123 K under steam atmosphere

Figure 5

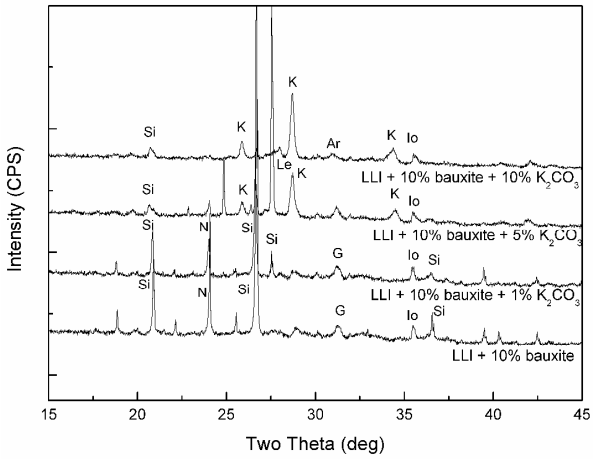

（Si - Silicon oxide (SiO_2); Io - Iron oxide (Fe_3O_4); K – Kaliophilite ($KAlSiO_4$); N - Nosean ($Na_{8.08}(Al_6Si_6O_{24})(SO_4)_{0.98}$); G - Gehlenite ($Ca_2Al(AlSi)O_7$); Ar – Arcanite ($K_2SO_4$); Le - Leucite ($KAlSi_2O_6$)）

Figure 5 The XRD patterns of the ashes of LLI lignite with 10 wt% bauxite additive produced by different concentrations of K_2CO_3 catalytic gasification at 1123 K under steam atmosphere

Figure 6

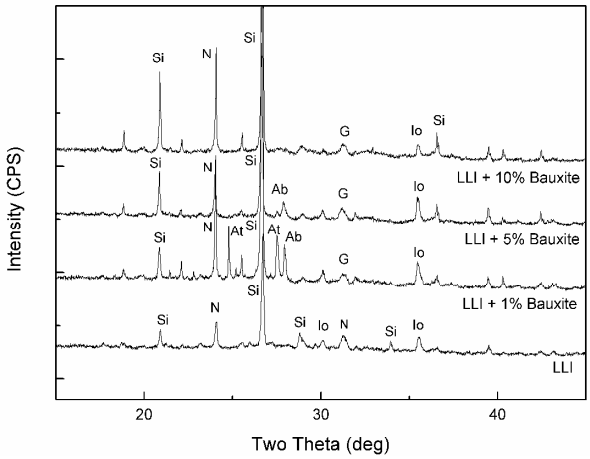

（Si - Silicon oxide (SiO_2); Io - Iron oxide (Fe_3O_4); N - Nosean ($Na_{8.08}(Al_6Si_6O_{24})(SO_4)_{0.98}$); At - Anorthoclase ($(Na,K)(Si_3Al)O_8$); Ab - Albite ($NaAlSi_3O_8$); G - Gehlenite ($Ca_2Al(AlSi)O_7$)）

Figure 6 The XRD patterns of the ashes of LLI lignite with different concentrations of bauxite additive produced by gasification at 1123 K under steam atmosphere

Figure 7

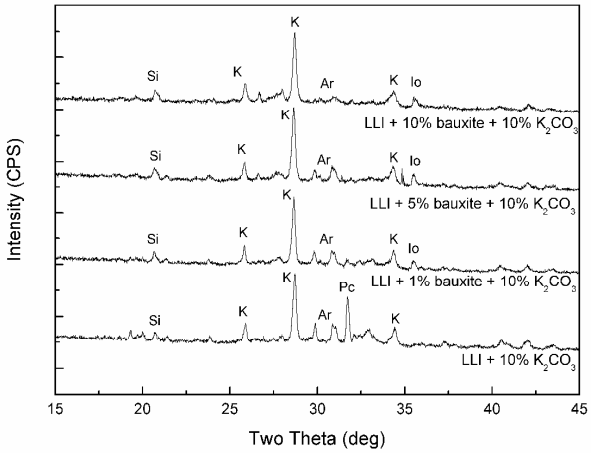

（Ar – Arcanite (K_2SO_4); Si - Silicon oxide (SiO_2); Io - Iron oxide (Fe_3O_4);

K – Kaliophilite ($KAlSiO_4$); Pc – Potassium calcium silicate ($K_4CaSi_3O_9$)）

Figure 7 The XRD patterns of the ashes of LLI lignite with different concentrations of bauxite additive produced by catalytic gasification with 10wt% K_2CO_3 at 1123 K under steam atmosphere